Sensing and Bio-Sensing Research 51 (2026) 100942

Contents lists available at ScienceDirect

Sensing and Bio-Sensing Research

journal homepage: www.elsevier.com/locate/sbsr

One-step Pd-NPs/Tyrosinase/Nafion biosensor for dopamine detection in the low μM range: ORR interference, defect-rich surface chemistry effects, and sensing pathway differentiation

M. Koch [a], H. Caparrotti [b], C. Pauly [c], O. Janka [d], M. Erzina [e], Y.E. Silina [b,*]

[a] HTW Saar – University of Applied Sciences, Saarbrücken, Germany
[b] Saarland University, Institute of Biochemistry, Saarbrücken, Germany
[c] Saarland University, Core Facility CoMiTo, Department of Materials Science, Saarbrücken, Germany
[d] Saarland University, Inorganic Solid State Chemistry, Saarbrücken, Germany
[e] University of Chemistry and Technology, Department of Solid State Engineering, Prague, Czech Republic

ARTICLE INFO

Keywords:
Electrodeposited Pd-NPs
Pd-oxides
ORR
Dopamine
Indirect redox reaction
One-step biosensor

ABSTRACT

A one-step (OS) biosensor for low micromolar (μM) dopamine (DA) detection was developed *via* co-electrodeposition from multiple palladium-based electrolyte containing tyrosinase (Tyr) and Nafion (Naf). The resulting OS biosensor modified with hybrid Pd-NPs/Tyr/Naf layer enabled DA detection in synthetic urine below 10 μM, with recovery rates of ~98–112 %.

A key challenge was signal interference caused by indirect redox reactions between Pd-oxides (present on the surface of the electrodeposited Pd-NPs) and free DA, as well as from the oxygen reduction reaction (ORR). This issue was addressed by promoting the formation of non-stoichiometric PdO_x ($x < 1$) through mild heating of the electrolyte during electrodeposition. This defect-rich surface suppressed ORR and non-enzymatic, ORR-mediated DA interactions, while retaining the catalytic activity of Pd-NPs toward dopamine-quinone as an enzymatic product.

Beyond its practical value, this work provides a framework for the controlled synthesis of OS-designed biosensing layers for enzymatic neurotransmitter detection at low μM levels, while minimizing interference from the intrinsic catalytic activity of electrodeposited Pd-NPs.

1. Introduction

A one-step (OS) methodology enabling the electrodeposition of biosensing layers onto the surface of screen-printed electrodes (SPEs) from multiple electrolytes, first proposed several years ago, has emerged as a promising alternative to conventional layer-by-layer (LbL) drop-coating approaches. [1,2] This methodology offers several key advantages, including the formation of highly reproducible and homogeneous nano-dimensional sensing layers that are both mechanically and chemically stable. It also prevents the rapid elution of the biosensing layer (comprising enzymes and binding polymer agents) and eliminates diffusion-limited processes. [1,2]

Importantly, the OS methodology enables the electrodeposition of oxidases (a class of enzymes that function *via* oxygen consumption) in their intact, bioactive form. The platform has proven effective for immobilizing oxidases with isoelectric points (pI) ranging from ~4.2 to ~5.8, including: glucose oxidase (GOx, *Aspergillus niger*, pI ≈ 4.2), lactate oxidase (LOx, *Aerococcus viridans*, pI ≈ 4.3), and alcohol oxidase (AOx, *Pichia pastoris*, pI ≈ 5.4–5.8). [3] This approach enables the fabrication of biosensors for monitoring and analyzing of glucose, lactate, and alcohols within the millimolar (mM) concentration range.

However, extending this OS approach to the detection of analytes in the low micromolar (μM) range remains a significant challenge. For instance, despite successful *co*-electrodeposition of uricase with copper nanoparticles (NPs) and a polymer matrix, detecting uric acid below 50 μM proved difficult. [4] This limitation is likely attributable to the high

Abbreviations: Pd-NPs, palladium nanoparticles; SPEs, screen-printed electrodes; OS, one step electrodeposition; LbL, layer by layer; Tyr, Tyrosinase; Naf, Nafion; SEM, scanning electron microscopy; HR-TEM, High-Resolution Transmission Electron Microscopy; PXRD, Powder X-ray diffraction; CV, cyclic voltammetry; CP, chronopotentiometry; ORR, oxygen electroreduction reaction; DA, dopamine; BQ, p-benzoquinone.

* Corresponding author at: Institute of Biochemistry, Saarland University, Campus B 2.2, Room 317, Saarbrücken, Germany.
E-mail address: yuliya.silina@uni-saarland.de (Y.E. Silina).

https://doi.org/10.1016/j.sbsr.2025.100942
Received 19 October 2025; Received in revised form 8 December 2025; Accepted 10 December 2025
Available online 11 December 2025

catalytic activity of electrodeposited NPs, whose surface oxides may engage in unintended redox interactions with target analytes, interfering with the enzymatic signal. [4–6] In other words, at low μM analyte levels, NPs may react not only with enzymatic products but also directly with the analyte/substrate itself.

Meanwhile, many physiologically relevant analytes, particularly neurotransmitters such as glutamate, dopamine (DA), serotonin, adrenaline, and norepinephrine, must be detected at very low μM or sub-μM concentrations. For example, DA levels in biological fluids typically range from nanomolar to <10 μM making reliable low-level detection crucial for neurological and clinical research. [7–9] More importantly, non-enzymatic interactions between DA and electrocatalytic NPs in the absence of a specific enzyme compromise the specificity and selectivity of its detection, an especially critical concern when analyzing complex media. [10]

Tyrosinase (Tyr), an oxidase with a pI of ~4.4–4.9 [11], is commonly used in DA biosensors due to its ability to selectively bind and oxidize catecholamines to *o*-quinones in the presence of oxygen, offering greater specificity than non-enzymatic sensing. [12–17] However, the conventional LbL drop-coating approach for Tyr immobilization often suffers from poor film uniformity, enzyme loss, and limited reproducibility. [18,19] As a result, alternative strategies, such as the one-step electrodeposition method, are needed for more stable and reliable fabrication of Tyr-based electrochemical biosensors. [20]

Here, we report the development of a one-step (OS) designed biosensor produced from multiple electrolyte containing palladium precursors, tyrosinase (Tyr), and Nafion. The resulting biosensor based on hybrid electrodeposited palladium nanoparticles (Pd-NPs), Tyr and Nafion (Pd-NPs/Tyr/Naf) enables DA detection in synthetic urine at concentrations below 10 μM.

During the study, indirect non-enzymatic redox interactions between conventional Pd-oxides and free DA, as well as interference from the oxygen reduction reaction (ORR), were identified. These issues were addressed by promoting the formation of non-stoichiometric Pd-oxides on the electrode surface. This modification effectively suppressed both ORR and undesired redox interactions between Pd-NPs (functioning as electrocatalysts within the biosensing layer) and DA, while preserving catalytic activity toward dopamine-quinone, the enzymatic reaction product.

The novelty of this study lies in several key findings: (*i*) the impact of defect-rich surface chemistry on the activity of electrodeposited Pd-NPs in the oxygen reduction reaction (ORR), while maintaining constant lattice parameters; (*ii*) the defined influence of molecular oxygen adsorption on defect-rich electrodeposited Pd-NPs in both ORR and indirect redox interactions with dopamine (DA); (*iii*) the identification of an indirect redox reaction of DA on Pd-NPs, leading to non-enzymatic DA conversion; (*iv*) the established activity of defect-rich electrodeposited Pd-NPs contained non-stochiometric PdO_x ($x < 1$) toward dopamine-quinone (the enzymatic reaction product); (*v*) the optimized design of a hybrid biosensing layer with Tyr for enzymatic DA detection in the low μM range; (*vi*) and the clear differentiation between non-enzymatic and enzymatic DA conversion pathways on the surface of electrodeposited Pd-NPs.

2. Experimental part

2.1. Chemicals and Materials used in this study are provided in the ESI

2.1.1. Preparation of Pd-NPs-modified electrodes (Electrode 1 and Electrode 2)

To investigate the specific role of the electrocatalyst (palladium nanoparticles, Pd-NPs) in the electrochemical redox reactions with dopamine (DA), the following model experiment was performed. Pd-NPs were electrodeposited from a Pd-electrolyte solution (pH 9.3) onto the surface of screen printed electrodes modified with graphene oxide (SPEs/GO), following a previously optimized protocol. [2] Briefly, 10 μL of the Pd-electrolyte at room temperature (20 ± 2 °C) was dropped onto the working electrode (GO), followed by cathodic electrodeposition at −2.5 mA for 30 s (*Electrode 1*). For comparison, a second design of the electrode (*Electrode 2*) was prepared under identical conditions, except the electrolyte was preheated to 40 ± 5 °C prior to electrodeposition. The cathodic current and deposition time were kept constant in both cases.

2.2. Fabrication of electrodes modified with one-step (OS) hybrid biosensing Pd-NPs/Tyr/Naf layer (hybrid Electrode 1 and hybrid Electrode 2)

Hybrid electrodes incorporating tyrosinase (Tyr), Nafion (Naf), and Pd-NPs were fabricated using a single-step (one-step, OS) co-electrodeposition approach, in which all components were deposited simultaneously. [3] Briefly, the Pd-electrolyte was premixed with 2 % Naf and 11 mg/mL Tyr solutions in a 1:1:1 (*v/v/v*) ratio, and electrodeposition was carried out from this multiple electrolyte under the same conditions used for individual Pd-NPs deposition (−2.5 mA, 30 s). Two batches of OS-modified electrodes were produced: *Hybrid Electrode 1* using room temperature (20 ± 2 °C) and *Hybrid Electrode 2* using a pre-heated multiple electrolyte (40 ± 5 °C). All electrodes were prepared in at least triplicate, and their performance was evaluated using statistical analysis (mean ± SD).

2.3. Electrochemical characterization

All electrodes, regardless of design, were characterized by cyclic voltammetry (CV) using a one-channel PalmSens4 (PalmSens, Utrecht, The Netherlands) potentiostat at a scan rate of 50 mV/s. To avoid direct non-enzymatic oxidation of dopamine [21] and to prevent additional Pd-oxide formation on the surface of Pd-NPs during cycling, both of which occur in the anodic potential range, all electrodes were scanned within a restricted potential window of −0.4 V to 0 V, unless otherwise specified.

To verify the amount of electrodeposited Pd-NPs, either individual (*section 2.2*) or in a hybrid layer (*section 2.3*) form as a function of synthesis temperature, the nanoparticles were dissolved in a 1 M HCl droplet in chronopotentiometric mode (CP) at a constant current of −0.5 mA for 200 s. [22]

2.4. Oxygen mini-sensor studies

a) Study of oxygen adsorption on the surface of electrodeposited Pd-NPs. To compare oxygen adsorption on Pd-NPs deposited at room temperature (*Electrode 1*) and 40 ± 5 °C (*Electrode 2*), an OXR430 fiber-optic oxygen minisensor (PyroScience GmbH, Aachen, Germany) was utilized. The sensor needle was placed in a buffer droplet on the Pd-NPs-modified SPE/GO and oxygen concentration (μmol/L) was recorded during electrode polarization using PyroScience software.

b) Evaluation of Tyrosinase (Tyr) activity in a solution. Biochemical transformation of DA to dopamine-o-quinone catalysed by tyrosinase (Tyr) is accompanied by oxygen consumption [23,24]:

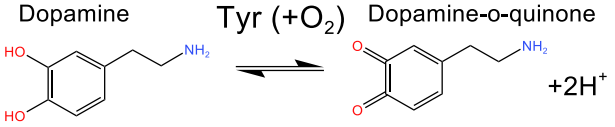

(1)

Therefore, Tyr activity was assessed by monitoring oxygen consumption during its reaction with DA. An OXR430 fiber-optic oxygen minisensor was inserted in a 150 μL droplet of 1 mM DA, after which 10 μL of Tyr solution (11 mg/mL) was added; oxygen depletion was recorded without applied polarization. Active Tyr typically reduces oxygen by 0–30 μmol/L within 100 s (see ESI, Fig. S1, shown for the

intact Tyr solution). The same procedure was used to test Tyr after mixing with Pd-electrolyte and Nafion (Naf), confirming that its biochemical activity remained preserved (ESI, Fig. S2).

c) Tyr activity after co-deposition with Pd-NPs and Naf (*hybrid Electrodes 1* and *2*). Using the same oxygen minisensor approach as in (*a*) and (*b*), Tyr activity within the co-deposited Pd-NPs/Tyr/Naf hybrid layer was evaluated. A droplet of μM-level DA was placed onto the hybrid-modified electrode. The minisensor needle was inserted into the droplet, and polarization was applied.

According to formula (*1*), if Tyr remains active after co-deposition, oxygen consumption in the presence of DA increases relative to the buffer (ESI, Fig. S3). The enzymatically formed reaction product, quinone, is then reduced at the Pd-NPs on the hybrid sensing layer, generating the electrochemical signal measured in CV mode.

2.5. Scanning electron microscopy (SEM) and transmission electron microscopy (TEM) investigations

SEM images of individual and hybrid electrodeposited Pd-NPs-based sensing layers were made on a JEOL JSM-6460LV Scanning Electron Microscope equipped with an Oxford INCA X-ray spectral analysis system, at an accelerating voltage of 15 keV. The image size was 1280 × 960 pixels.

To study the crystallinity of electrodeposited layers, a set of TEM studies of Pd-NPs-modified SPEs were conducted. Briefly, small pieces of the Pd-NPs-based sensing layers were scratched using sandpaper P180, dispersed in a water droplet and placed on a 400 mesh carbon film grid (MicroToNano, Haarlem, The Netherlands, type 22-1MC040–50). Bright field HR-TEM images were obtained at 200 kV accelerating voltage using a JEOL (Akishima, Tokio, Japan) JEM-F200 microscope.

2.6. Powder X-ray diffraction (PXRD)

Powder XRD patterns of the GO electrodes modified with Pd-NPs were recorded at room temperature using an X'Pert MPD diffractometer (PANalytical, Netherlands) in Bragg-Brentano θ-θ geometry (Cu $K\alpha_{1,2}$ radiation; $\lambda_1 = 154.06$ pm, $\lambda_2 = 154.44$ pm; 12 μm Ni Kβ filter; PIXcel1D detector). Measurements were performed over a 2θ range of 7–120° with a 0.013° step size and 4 h total scan time. Data were analyzed using the Bruker TOPAS 5.0 software: electrode reflections were fitted as individual peaks, while Pd-NPs were fitted as a structure with initial parameters. [25] Crystallite sizes were calculated using the LVol-IB model.

2.7. RAMAN study

The surface chemistry of electrodeposited Pd-NPs was investigated using a LabRAM HR Evolution (HORIBA) spectrometer equipped with a 532 nm He-Ne laser (3 mW, Melles Griot, IDEX Optics and Photonics, Albuquerque, NM, USA). The measurement time was set to 20 s, and each spectrum represented an average of 6 scans.

2.8. Analysis of urine-spiked samples

To evaluate the analytical performance of electrodes modified with OS hybrid biosensing Pd-NPs/Tyr/Naf layers, dye-free Sigma matrix urine was spiked with known low concentrations of standard DA solutions, and calibration curves were constructed. The concentration of spiked DA was determined using the external standard approach to assess recovery rates.

3. Results and discussion

3.1. Characterization of electrodes modified with Pd-NPs and investigation of their activity in the oxygen reduction reaction (ORR)

a) Morphological and Electrochemical Characterization.

In the first set of experiments, SPEs modified with individual Pd-NPs electrodeposited at 20 ± 2 °C (*Electrode 1*) and 40 ± 5 °C (*Electrode 2*) were investigated. It is hypothesized that slight variations in the synthesis temperature of electrodeposited Pd-NPs may influence their physicochemical properties, such as morphology or density, crystallographic structure, and surface chemistry, which, in turn, affect their electrocatalytic activity.

SEM and HR-TEM analyses revealed similar particle size (20–60 nm), density, and morphology for both electrodes, with polyhedral shapes and clear lattice fringes indicating high crystallinity (Fig. 1A,B,D,E). No notable agglomeration of Pd-NPs was observed. Chronopotentiometric dissolution further confirmed comparable Pd-NPs loading, as both electrodes exhibited nearly identical CP curves (Fig. 1C,F), with dissolution occurring between ~90–125 s. These findings confirm that Pd-NPs morphology and density were not significantly affected by the synthesis temperature.

Despite identical morphology and density of Pd-NPs on the surface of both electrodes, their behavior with oxygen was different, Fig. 2. Thus, Pd-NPs produced at room temperature (*Electrode 1*) exhibited higher ORR activity at pH 5.5 ± 0.2 (larger cathodic peak current, Fig. 2A, *solid line*) compared to Pd-NPs synthesized at 40 ± 5 °C (*Electrode 2, dashed line*). However, Pd-NPs synthesized at 40 ± 5 °C (*Electrode 2*) exhibited higher oxygen consumption (Fig. 2B *dashed lines*) *vs.* Pd-NPs synthesized at room temperature (*Electrode 1, solid line*). The same trend was observed during testing of both electrodes over an extended scan range (ESI, Fig. S4).

This observation can be explained by the fact that, at higher synthesis temperatures, Pd-NPs may form surfaces where O_2 binds too strongly, leading to active site poisoning during the ORR. Alternatively, Pd-NPs synthesized at 40 ± 5 °C may exhibit electronic states that are less favourable for O-O bond cleavage, potentially due to strain, size effects, or the formation of oxidized species, which alters their interaction with oxygen. The observed results related to strong oxygen adsorption on Pd-NPs align with the well-established fact that, in acidic media, Pd electrocatalysts suffer from strong oxygen binding, which affects their ORR activity. [26,27]

More importantly, different activity on both electrodes in ORR may significantly impact electrocatalytic properties of Pd-NPs in redox reaction with a target electroactive analyte, such as dopamine (*see section 3.2*).

b) Surface and Structural Properties.

A previous study has shown that variations in Pd lattice parameters can influence ORR activity. [28] To investigate the role of the crystal structure and surface chemistry on Pd-NPs' electrocatalytic activity, PXRD and RAMAN analyses were conducted. Although Pd-NPs synthesized at 20 °C were hypothesized to expose more active facets (*e.g.*, Pd (111)), the performed PXRD revealed no significant difference in the facet ratios between samples (1.59 ± 0.06 *vs.* 1.58 ± 0.08), with nearly

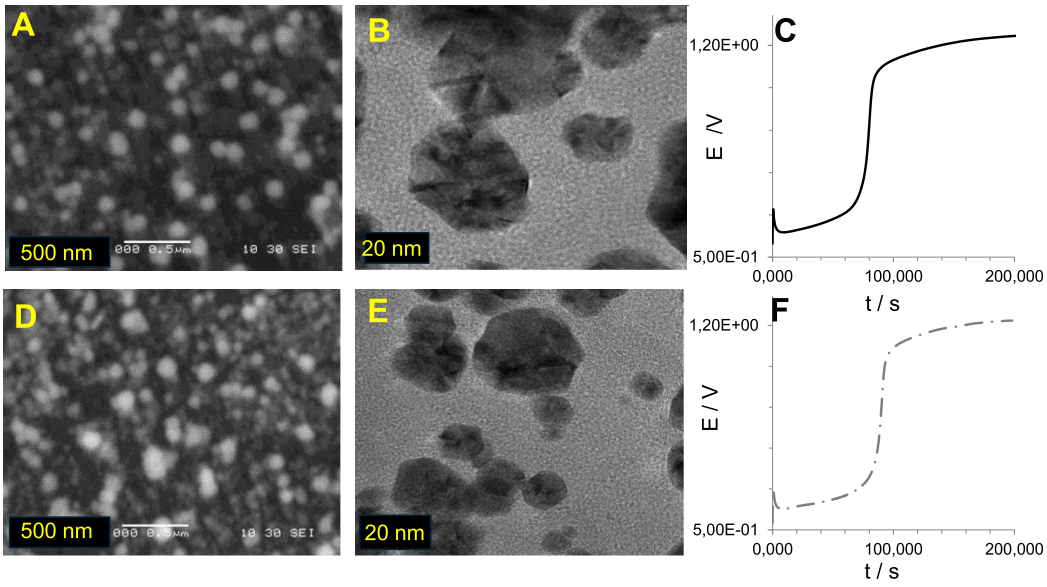

Fig. 1. SEM (A,D), TEM (B,E) images and CP dissolution plots (C,F) recorded from *Electrode 1* (A,B,C) and *Electrode 2* (D,E,F) modified with electrodeposited Pd-NPs.

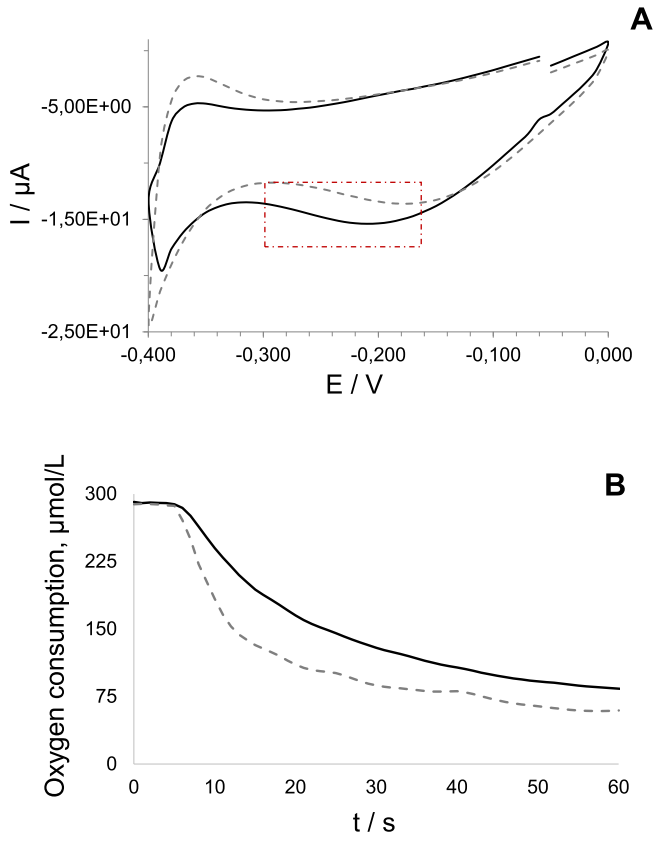

Fig. 2. CV plots (A, *2d scans shown*) and dynamic oxygen minisensor responses (B) recorded in a droplet of a background solution (pH 5.5 ± 0.2) at 50 mV/s from −0.4 V to 0 V *vs.* Ag/AgCl: from the SPEs modified with Pd-NPs deposited at 20 ± 2 °C (*Electrode 1*, *solid lines*) and 40 ± 5 °C (*Electrode 2, dashed lines*). *Note:* the electrochemical read-out in the CVs plots is highlighted by a red dotted square.

identical spectra (Fig. 3A, see also Table S1). Therefore, the differences in ORR activity between *Electrode 1* and *Electrode 2* (see Fig. 2) cannot be attributed to their crystallographic structure.

In contrast, the surface chemistry of both electrodes was different. Briefly, RAMAN spectra recorded from the *Electrode 1* (20 ± 2 °C) exhibited an intense band at 640 cm^{-1} assigned to PdO, Fig. 3B (*red spectra*).

Notably, when the deposition temperature is increased to 40 ± 5 °C (*Electrode 2*), the PdO band shifts from 640 cm^{-1} to 629 cm^{-1}, accompanied by the appearance of a shoulder at approximately 617 cm^{-1}, Fig, 3B (*blue spectra*). This intensive peak with the shoulder is more likely attributed not to conventional PdO, but to adsorbed oxygen species (*O) on Pd surfaces, *viz.* the amorphous or non-stoichiometric PdO_x ($x < 1$) species, highly disordered Pd-O bonds, hydroxylated surfaces (Pd–OH), or chemisorbed oxygen species. [29–31] These observations suggest a defect-rich surface on *Electrode 2*.

In summary, although both electrodes exhibited a similar morphology of Pd-NPs, loading, crystallinity and lattice strain (Table S1) their surface chemistry varied remarkably. Unlike *Electrode 1*, *Electrode 2* featured non-stoichiometric, defect-rich Pd oxides. Such changes in surface electronic structure can influence electron transfer, conductivity, and oxygen adsorption – factors that critically affect electrocatalytic performance.

3.2. The impact of defect-rich surface chemistry of electrodeposited Pd-NPs on their activity in redox reactions with dopamine (DA)

The defect-rich surface chemistry of electrodeposited Pd-NPs, which was shown to influence their ORR activity (*see above*), was hypothesized to also affect their electrocatalytic behavior toward target analytes. This hypothesis was tested in a model experiment using dopamine (DA) as a representative analyte.

Notably, Pd-NPs synthesized at room temperature (*Electrode 1*), which previously demonstrated enhanced activity in the ORR (*see section 3.1*, Fig. 2), also exhibited significant activity in redox interactions with DA, as shown in Fig. 4A (*dashed line*). A marked increase in cathodic current was observed even at low DA concentrations (indicated by the arrow), suggesting a strong interaction. This current response can be explained by an indirect redox interaction (catalytic effect) between the palladium surface and DA in the presence of ORR, rather than through classical direct electrooxidation pathways. [32,33] Thus, *Electrode 1* enables a non-enzymatic transformation of DA, occurring independently of tyrosinase (Tyr) involvement.

In contrast, defect-rich Pd-NPs (*Electrode 2*), which exhibit lower ORR activity, were also electrochemically inactive in redox reactions

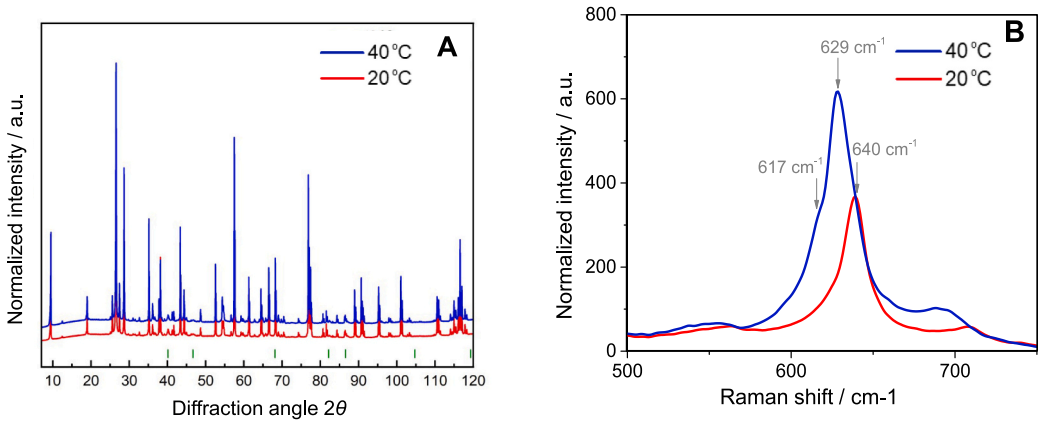

Fig. 3. X-Ray diffraction patterns (A) and RAMAN (B) spectra recorded from *Electrode 1* (Pd-NPs deposited at room temperature, 20 ± 2 °C, *red spectra*) and *Electrode 2* (Pd-NPs deposited from a preheated electrolyte, 40 ± 5 °C, *blue spectra*). *Note:* the X-Ray diffraction patterns are offset for better visibility. The green ticks in XRD patterns indicate the Bragg positions for elemental Pd. (For interpretation of the references to colour in this figure legend, the reader is referred to the web version of this article.)

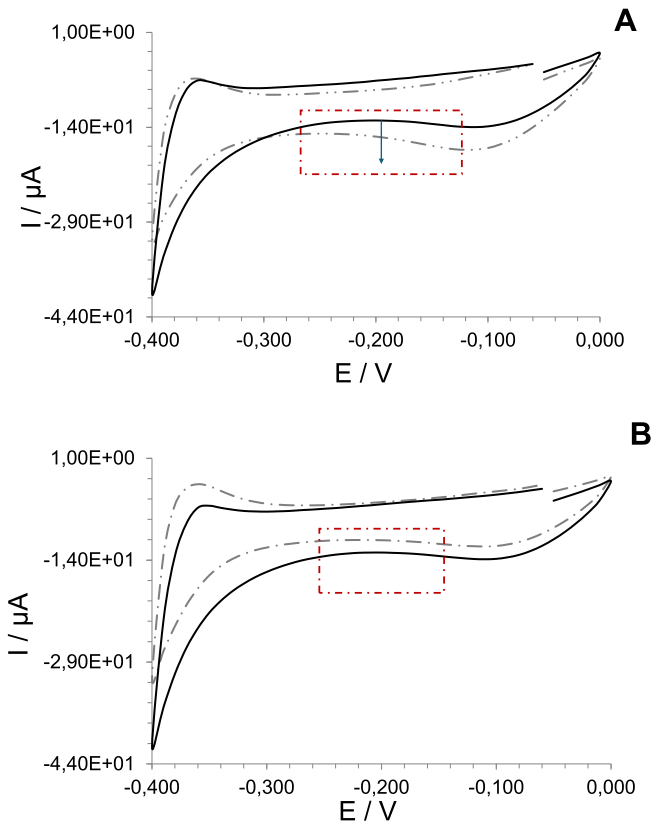

Fig. 4. CV plots (2[d] *scans shown*) recorded in a droplet of a background solution (*solid lines*), and 10 µM DA (*dashed lines*) at 50 mV/s from the SPEs/GO modified with Pd-NPs deposited at 20 ± 2 °C (A) and at 40 ± 5 °C (B). *Note:* pH of all solutions was 5.5 ± 0.2. The read-out region in the CVs is highlighted by a dotted square.

with DA under the same experimental conditions, Fig. 4B (no increase in cathodic current was observed in the presence of DA).

In other words, although Pd is a well-known catalyst for oxygen reduction, our results demonstrate how the ORR activity of Pd electrodes affects redox reactions involving DA. In particular, the defect-rich Pd-NPs (*Electrode 2*) suppress ORR, thereby minimizing competing non-enzymatic, indirect DA transformation. This suppression can improve enzymatically driven DA sensing by preventing ORR-mediated indirect DA reactions.

In the context of biosensor development, the above demonstrated results suggest that a sensing layer incorporating tyrosinase (Tyr) and Pd-NPs electrodeposited at room temperature (*Electrode 1*) may exhibit at least two competing and simultaneous DA conversion pathways: (*i*) indirect redox interaction (non-enzymatic) and (*ii*) biochemical (enzymatic, supported by Tyr). This overlap could lead to inaccurate data interpretation.

Indeed, *Electrode 1* showed a strong and linear response to free DA at µM concentrations, even in the absence of the specific enzyme (Table 1), highlighting a dominant indirect non-enzymatic pathway (*i*) for DA conversion. This suggests that the presence of these electrodeposited Pd-NPs (*Electrode 1*) in the hybrid biosensing layer containing enzyme Tyr may lead to undesirable background signals and therefore should be avoided.

In contrast, *Electrode 2* modified with defect-rich and less active in ORR Pd-NPs exhibited no measurable response to free DA within the same concentration range (Table 1), indicating effective suppression of indirect redox interaction.

These findings allow to suggest that when the enzyme (*e.g.*, Tyr) is incorporated into a biosensing layer containing defect-rich and less active in ORR Pd-NPs (*Electrode 2*), the observed response is predominantly governed by the enzymatic biochemical reaction (*ii*) and no interfering electrocatalytic contribution from the electrodeposited nanoparticles is expected (*see section 3.4*).

3.3. Distinguishing between oxygen reduction and quinone reduction in the cathodic range on electrodeposited Pd-NPs

Even beyond the competing indirect redox interaction (electrochemical non-enzymatic) (*i*) and biochemical (enzymatic) pathways (*ii*) occurring on the surface of electrodeposited Pd-NPs in the presence of DA, the reliability of read-outs associated with the reduction of the reaction product (quinone) remains questionable. Under ambient conditions, the use of Pd-NPs for quinone reduction is particularly challenging due to interference from the oxygen reduction (ORR). Since both oxygen and quinones are reduced at similar cathodic potentials, their overlapping electrochemical signals can hinder accurate detection on Pd-NPs-based electrodes.

Table 1
Analytical performance of *Electrode 1* and *Electrode 2* recorded at −0.25 V in model DA solutions (pH 5.5 ± 0.2).

System	Calibration formula	R^2	Sensitivity μA·μM^{-1}·cm^{-2}	LDR, μM	DA added, μM	DA found, μM	Recovery, %
Electrode 1	y = −0.557·x − 9.2	0.992	1.833	0–5	2	2.13	106.5
					5	5.05	100.5
Electrode 2	y = −0.042·x − 10.0	0.042	–	–	–	–	–

For example, *Electrode 1* is highly active toward ORR (Fig. 2, *solid plots*), which may dominate the cathodic current under oxygen-rich conditions. As a result, it becomes difficult to distinguish whether the observed current arises from quinone reduction (*a*), oxygen reduction (*b*), or a combination of both (*c*). Furthermore, the background cathodic current generated by ORR can mask or distort the signal associated with quinone reduction, particularly at low quinone concentrations. This competition can result in overlapping signals and misinterpretation of redox behavior, issues that are especially problematic in biosensing applications, where selectivity and sensitivity are critical.

This hypothesis was confirmed during the next set of experiments. *Electrode 1* and *Electrode 2* modified with electrodeposited Pd-NPs were tested in model quinone solutions (p-benzoquinone, BQ, used as a case study).

As expected, an increase in the μM range of BQ concentration led to a decrease in the cathodic current recorded from *Electrode 1* (Fig. 5A). This effect is most likely due to increased competition between ORR and BQ reduction for the same active catalytic sites present on the Pd-NPs.

As a result, the use of Pd-NPs produced at room temperature and containing conventional PdO on the surface (Fig. 3B, *Electrode 1*) in a biosensing layer with tyrosinase (Tyr), under ambient conditions, appears unreliable for enzymatic DA detection. Firstly, these Pd-NPs support a competing indirect redox interaction with DA and the appearance of an interfering cathodic current (Fig. 4A). Secondly, the cathodic signal corresponding to the reduction of the enzymatic reaction product (quinone) overlaps with competing oxygen reduction processes.

In contrast, *Electrode 2*, featuring a surface enriched with defect-rich Pd oxides (Fig. 3B), exhibited a linear cathodic response to increasing quinone concentrations in the presence of oxygen (Fig. 5B). A slight but consistent shift of the cathodic peak toward more negative potentials was observed with rising μM quinone concentrations. This behavior agrees with previous reports attributing such shifts to quinone adsorption and increased surface coverage, affecting electron-transfer kinetics and the local electrode environment. [34]

In summary, the defect-rich surface chemistry of Pd-NPs (*Electrode 2*) re-presented by non-stochiometric Pd-oxides and lacking activity in both ORR and indirect redox reactions with low DA concentrations, is electrocatalytically active toward quinones – the enzymatic oxidation products of DA with Tyr, (see reaction (*1*)). This behavior minimizes non-specific signals and enhances Tyr-specific response.

From a practical standpoint, these results demonstrate that Pd-NPs electrodeposited exclusively at 40 ± 5 °C (*Electrode 2*) can serve as an effective component in constructing a hybrid biosensing layer for enzymatic DA detection at μM concentration level (*see the next section)*.

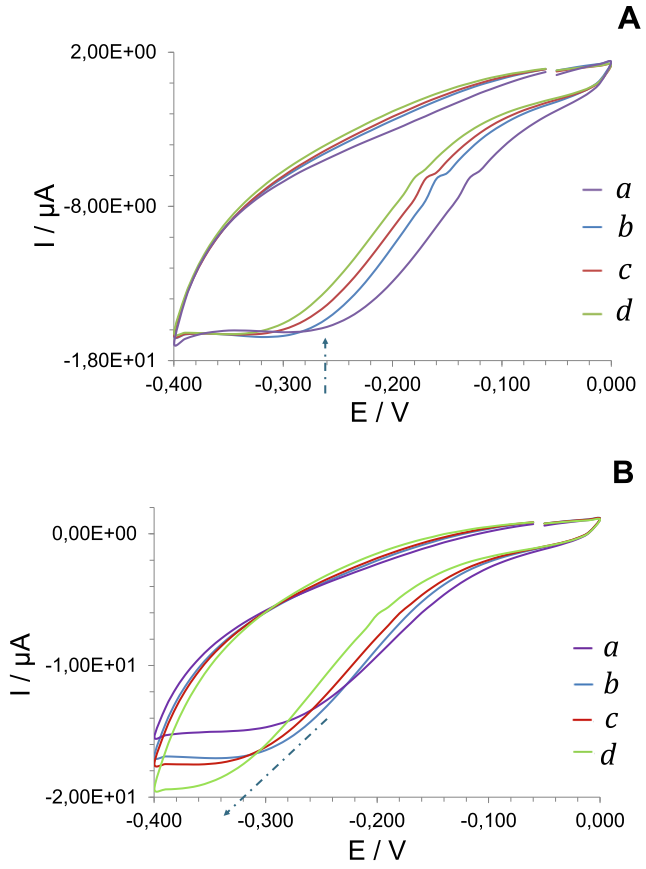

Fig. 5. CV plots (2nd scans shown) recorded at 50 mV/s from −0.4 V to 0 V (*vs.* Ag/AgCl) using *Electrode 1* (A) and *Electrode 2* (B) modified with Pd-NPs deposited at 20 ± 2 °C (A) and at 40 ± 5 °C (B). The applied BQ concentrations (pH 5.5 ± 0.2) were as follows: (a) 0 μM, (b) 1 μM, (c) 3 μM, (d) 5 μM.

3.4. Toward controlled synthesis of the hybrid biosensing layer for enzymatic detection of DA

Furthermore, the design of *Electrodes 1,2* modified with individual Pd-NPs, was altered by incorporating the enzyme tyrosinase (Tyr) and the binding agent Nafion (Naf) into the Pd-electrolyte (see *Experimental section* for details). Briefly, electrodeposition from this multiple electrolyte was carried out at −2.5 mA for 30 s: at room temperature for the formation of *hybrid Electrode 1* (exhibiting conventional PdO), and at 40 ± 5 °C for defect-rich (PdO_x) *hybrid Electrode 2*.

The presence of a bioorganic component in the Pd-electrolyte reduced the size of the resulting Pd-NPs from 20 to 60 nm to 10–20 nm (Fig. 6A,D), while preserving their crystallinity (Fig. 6B,E), as evidenced by the lattice fringes visible in TEM images.

Notably, the amount of deposited inorganic component (Pd-NPs) in the hybrid biosensing layer appears to be very similar in both systems studied. This is also supported by the CP curves, which show the onset of Pd-NPs dissolution at around 25 s, completing by 35 s (Fig. 6C,F). In other words, at first glance, similar to the individual Pd-NPs (see Fig. 1) no visible changes in the morphology or density of the hybrid Pd-NPs/Tyr/Naf layers were observed, regardless of the synthesis temperature used.

Importantly, for both electrodes modified with hybrid Pd-NPs/Tyr/Naf biosensing layers, the preserved biochemical activity of the co-deposited tyrosinase (Tyr) was confirmed through oxygen mini-sensor studies. Specifically, oxygen consumption on the surface of the hybrid layer increased with the concentration of DA applied (see *Experiment* and ESI, Fig. S3), indicating that biochemical pathway following reaction (*1*) occurred on both electrodes.

However, the electrochemical read-outs from the two electrodes were markedly different. No measurable response was recorded from *hybrid Electrode 1*, likely due to interference from the oxygen reduction reaction (ORR) and insensitivity to the reduction of the enzymatic product, ESI, Fig. S5. This means that even in the presence of

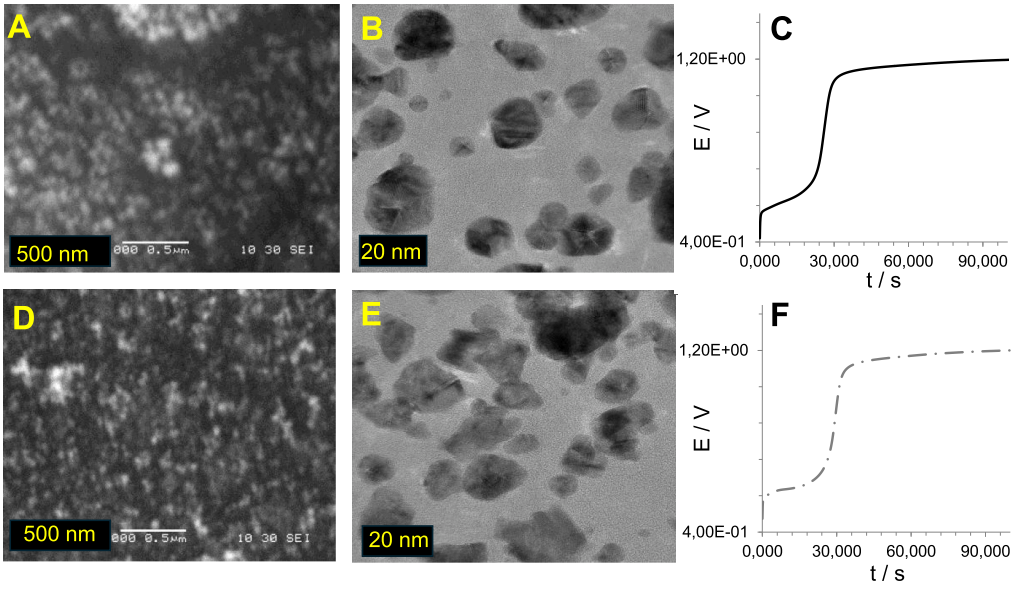

Fig. 6. SEM (A,D), TEM (B,E) images and CP dissolution plots (C,F) recorded from the SPEs modified with electrodeposited hybrid layers Pd-NPs/Tyr/Naf synthesized at 20 ± 2 °C (A,B,C) (*hybrid Electrode 1*) and 40 ± 5 °C (D,E,F) (*hybrid Electrode 2*).

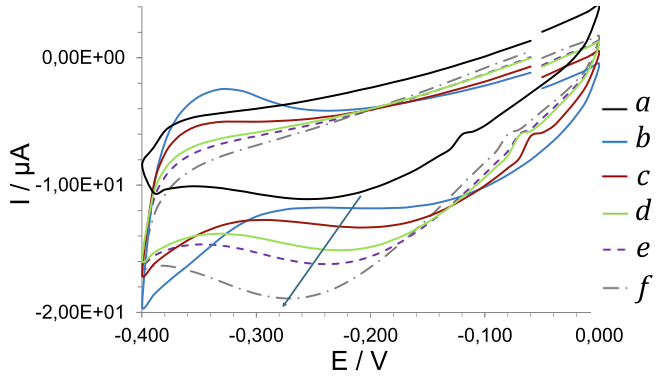

Fig. 7. CV plots (2nd scans shown) recorded at 50 mV/s from −0.4 V to 0 V (*vs.* Ag/AgCl) using *hybrid Electrode 2* modified with a Pd-NPs/Tyr/Naf layer deposited at 40 ± 5 °C. Dopamine (DA) concentrations: (a) 0 μM, (b) 1 μM, (c) 3 μM, (d) 5 μM, (e) 7 μM, and (f) 15 μM. The peak corresponding to formed quinone (as a product of enzymatic reaction between Tyr co-deposited in the hybrid layer and dropped DA) is indicated by an arrow.

immobilized Tyr with preserved biochemical activity on the surface of Pd-NPs synthesized at 20 ± 2 °C and despite the effective enzymatic reaction pathway it is not possible to record an electrochemical signal corresponding to quinone reduction, the product of DA enzymatic oxidation, from this hybrid electrode. The underlying reasons for this phenomenon are discussed in *sections 3.2* and *3.3*.

In contrast, *hybrid Electrode 2* produced at 40 ± 5 °C exhibited a linear increase in cathodic current corresponding to quinone reduction with increasing concentrations of applied DA, as shown in Fig. 7. The resulting linear dynamic range (LDR) in model buffered solutions was 1–15 μM, with a limit of detection (LOD) of 0.2 μM.

To explore the analytical capabilities of *hybrid Electrode 2* toward DA screening at μM level, next, its performance was tested in spiked urine samples. The biosensor provided a stable, linear response in the range of 0–5 μM, which is appropriate for detecting DA in biological fluids like urine.

The obtained recovery rates were ranged from ~98 % to 112 %, Table 2. Slight overestimation at 1 μM (112 % recovery) may be due to matrix effects but is within acceptable limits for preliminary applications.

To summarize, by controlling the surface chemistry of the inorganic component within hybrid biosensing layers on SPEs, it was possible to tune their electroanalytical performance in DA solutions. OS-designed biosensors with hybrid biosensing layers are easy to fabricate, handle, and through the clear distinction between enzymatic and non-enzymatic DA conversion simple to operate in μM concentration range with reliable electroanalytical signal readout.

4. Conclusions

Herein, a fundamental study demonstrating the exclusive role of defect-rich surface chemistry in governing the catalytic behavior of electrodeposited palladium nanoparticles (Pd-NPs) in the oxygen reduction reaction (ORR) and dopamine (DA) redox processes was conducted. More specifically, Pd-NPs with surface PdO, used as electrocatalysts in a hybrid biosensing layer containing tyrosinase and Nafion, exhibited unintended non-enzymatic electrocatalytic activity toward DA, thereby interfering with the enzymatic signal.

This non-enzymatic DA conversion *via* indirect ORR-mediated redox interaction with conventional PdO was effectively suppressed by introducing into the sensing layer non-stoichiometric PdO_x ($x < 1$), formed through mild heating of the electrolyte. This modification produced a

Table 2
Analytical performance of one-step (OS)-designed *hybrid Electrode 2* (Pd-NPs/Tyr/Naf layer was deposited at 40 ± 5 °C) recorded at −0.25 V in synthetic urine solutions spiked with DA (pH 6.3 ± 0.2).

System	Calibration formula	R^2	Sensitivity $\mu A \cdot \mu M^{-1} \cdot cm^{-2}$	LDR*, μM	DA added, μM	DA found, μM	Reco-very, %
Hybrid Electrode 2	y = −0.4543·x − 2.3	0.980	1.817	0–5	1	1.12	112
					3	2.95	98.3

* Linear detection range (LDR).

defect-rich surface with strong oxygen-binding properties, which reduced both the ORR and undesired indirect redox interactions with DA, while preserving activity toward dopamine-quinone, the enzymatic product. Importantly, these changes in catalytic behavior of electrodeposited Pd-NPs could not be attributed to variations in the crystallographic structure, morphology, or density of the Pd-NPs, confirming the dominant role of surface defect chemistry.

Overall, this work demonstrates a practical strategy for tuning the surface chemistry of OS-fabricated biosensors and offers a platform for reliable enzymatic detection of neurotransmitters in the low μM range.

CRediT authorship contribution statement

M. Koch: Visualization, Methodology, Investigation, Formal analysis. **H. Caparrotti:** Visualization, Methodology, Investigation, Formal analysis. **C. Pauly:** Methodology, Formal analysis, Data curation. **O. Janka:** Methodology, Investigation, Formal analysis. **M. Erzina:** Visualization, Methodology, Investigation, Formal analysis. **Y.E. Silina:** Conceptualization, Funding acquisition, Data acquisition, Methodology, Analysis, Validation, Writing – original draft.

Declaration of competing interest

The authors declare that they have no known competing financial interests or personal relationships that could have appeared to influence the work reported in this paper.

Acknowledgements

This study was carried out within the framework of the scientific program of **Y.E.S.** funded by the Deutsche Forschungsgemeinschaft (DFG, German Research Foundation, project 427949628).

O.J. acknowledges financial support from Saarland University and the German Science Foundation; Instrumentation and Technical Assistance for the powder X-ray diffraction measurements were provided by the Service Center X-ray Diffraction, with financial support from Saarland University and the German Science Foundation (project number INST 256/349-1).

C.P. acknowledges support from the CoMiTo core facility, Saarland University. HR-TEM funding was provided by the EU *via* the ERDF under the EFRE Saarland 2014-2020 program ("Investitionen in Wachstum und Beschäftigung").

Appendix A. Supplementary data

Supplementary data to this article can be found online at https://doi.org/10.1016/j.sbsr.2025.100942.

Data availability

Data will be made available on request.

References

[1] D. Semenova, K.V. Gernaey, B. Morgan, Y.E. Silina, Towards one-step design of tailored enzymatic nanobiosensors, Analyst 145 (2020) 1014–1024, https://doi.org/10.1039/c9an01745c.

[2] E.V. Butyrskaya, N. Korkmaz, E.V. Zolotukhina, et al., Mechanistic aspects of functional layer formation in hybrid one-step designed GOx/Nafion/Pd-NPs nanobiosensors, Analyst 146 (2021) 2172–2185, https://doi.org/10.1039/D0AN02429E.

[3] Y.E. Silina, One-step electrodeposited hybrid nanofilms in amperometric biosensor development, Anal. Methods 16 (2024) 2424–2443, https://doi.org/10.1039/d4ay00290c.

[4] M. Koch, Y.E. Silina, Uric acid detection by hydrogen peroxide independent biosensors: novel insights and applications, Microchem. J. 207 (2024) 112091, https://doi.org/10.1016/j.microc.2024.112091.

[5] E.V. Butyrskaya, N. Korkmaz, E.V. Zolotukhina, et al., Revealing the impact of surface composition of electrodeposited Cu and Ni nanoparticles on the specific electrooxidation of uric acid, Electrochim. Acta 538 (2025) 147012, https://doi.org/10.1016/j.electacta.2025.147012.

[6] E.V. Butyrskaya, E.V. Zolotukhina, P. Herbeck-Engel, et al., Toward the development of a specific non-enzymatic amperometric sensor for determining uric acid in fermentation samples, Microchim. Acta 192 (2025), https://doi.org/10.1007/s00604-025-06979-4.

[7] D. Caligiore, F. Giocondo, M. Silvetti, The neurodegenerative elderly syndrome (NES) hypothesis: Alzheimer and Parkinson are two faces of the same disease, IBRO Neurosci. Reports 13 (2022) 330–343, https://doi.org/10.1016/j.ibneur.2022.09.007.

[8] S.K. Arumugasamy, G. Chellasamy, S. Gopi, et al., Current advances in the detection of neurotransmitters by nanomaterials: an update, TrAC Trends Anal. Chem. 123 (2020) 115766, https://doi.org/10.1016/j.trac.2019.115766.

[9] B. Si, E. Song, Recent advances in the detection of neurotransmitters, Chemosensors 6 (1) (2018) 1–24, https://doi.org/10.3390/chemosensors6010001.

[10] R. Mondal, N. Mukherjee, S.F. Ahmed, A comprehensive review on the enzyme-free electrochemical dopamine sensing: development and challenges since inception, Inorg. Chem. Commun. 178 (2025) 114449, https://doi.org/10.1016/j.inoche.2025.114449.

[11] C.S. Mogilevsky, M.J. Lobba, D.D. Brauer, et al., Synthesis of multi-protein complexes through charge-directed sequential activation of tyrosine residues, J. Am. Chem. Soc. 143 (2021) 13538–13547, https://doi.org/10.1021/jacs.1c03079.

[12] T.G. Beatto, W.E. Gomes, A. Etchegaray, et al., Dopamine levels determined in synthetic urine using an electrochemical tyrosinase biosensor based on ZnO@Au core-shell, RSC Adv. 13 (2023) 33424–33429, https://doi.org/10.1039/d3ra06277e.

[13] J. Ahmed, M. Faisal, F.A. Harraz, et al., Development of an amperometric biosensor for dopamine using novel mesoporous silicon nanoparticles fabricated via a facile stain etching approach, Phys. E Low-Dimension. Syst. Nanostruct. 135 (2022) 114952, https://doi.org/10.1016/j.physe.2021.114952.

[14] K. Min, Y.J. Yoo, Amperometric detection of dopamine based on tyrosinase-SWNTs-Ppy composite electrode, Talanta 80 (2009) 1007–1011, https://doi.org/10.1016/j.talanta.2009.08.032.

[15] A. Liu, I. Honma, H. Zhou, Amperometric biosensor based on tyrosinase-conjugated polysacchride hybrid film: selective determination of nanomolar neurotransmitters metabolite of 3,4-dihydroxyphenylacetic acid (DOPAC) in biological fluid, Biosens. Bioelectron. 21 (2005) 809–816, https://doi.org/10.1016/j.bios.2005.03.005.

[16] I. Algov, A. Feiertag, R. Shikler, L. Alfonta, Sensitive enzymatic determination of neurotransmitters in artificial sweat, Biosens. Bioelectron. 210 (2022) 114264, https://doi.org/10.1016/j.bios.2022.114264.

[17] M. Florescu, M. David, Tyrosinase-based biosensors for selective dopamine detection, Sensors (Switzerland) 17 (6) (2017) 1314, https://doi.org/10.3390/s17061314.

[18] C. Lete, S. Lupu, B. Lakard, et al., Multi-analyte determination of dopamine and catechol at single-walled carbon nanotubes – conducting polymer – Tyrosinase based electrochemical biosensors, J. Electroanal. Chem. 744 (2015) 53–61, https://doi.org/10.1016/j.jelechem.2015.03.005.

[19] C. Tesoro, G. Cembalo, A. Guerrieri, et al., (2023) a critical overview of enzyme-based electrochemical biosensors for L-Dopa detection in biological samples, Chemosensors 11 (10) (2023) 523, https://doi.org/10.3390/chemosensors11100523.

[20] K. Jackowska, P. Krysinski, New trends in the electrochemical sensing of dopamine, Anal. Bioanal. Chem. 405 (2013) 3753–3771, https://doi.org/10.1007/s00216-012-6578-2.

[21] H. Caparrotti, Y.E. Silina, On the role of cysteamine modification of gold electrodes in redox reactions with dopamine, J. Appl. Electrochem. (2025), https://doi.org/10.1007/s10800-025-02378-y.

[22] S.A. Kleinikova, M.G. Levchenko, A.B. Yalmaev, et al., Some features of alcohols electrooxidation process on Pd, Rh and PdRh catalysts, Electrochim. Acta 409 (2022) 139998, https://doi.org/10.1016/j.electacta.2022.139998.

[23] C.A. Ramsden, P.A. Riley, Tyrosinase: the four oxidation states of the active site and their relevance to enzymatic activation, oxidation and inactivation, Bioorg. Med. Chem. 22 (2014) 2388–2395, https://doi.org/10.1016/j.bmc.2014.02.048.

[24] L. Ribovski, F.A. dos Santos, V. Zucolotto, B.C. Janegitz, Gold nanorods and poly (amido amine) dendrimer thin film for biosensing, J. Solid State Electrochem. 23 (2019) 1581–1591, https://doi.org/10.1007/s10008-019-04247-z.

[25] A.W. Hull, X-ray crystal analysis of thirteen common metals, Phys. Rev. 17 (1921) 571–588, https://doi.org/10.1103/PhysRev.17.571.

[26] C. Liang, S.-M. Xing, R. Zhao, et al., Pd/NiSix: an efficient and stable acid-ORR electrocatalyst, Chem. Catal. 4 (2024) 100849, https://doi.org/10.1016/j.checat.2023.100849.

[27] T. Wang, A. Chutia, D.J.L. Brett, et al., Palladium alloys used as electrocatalysts for the oxygen reduction reaction, Energy Environ. Sci. 14 (2021) 2639–2669, https://doi.org/10.1039/D0EE03915B.

[28] G. Bampos, L. Sygellou, S. Bebelis, Oxygen reduction reaction activity of Pd-based bimetallic electrocatalysts in alkaline medium, Catal. Today 355 (2020) 685–697, https://doi.org/10.1016/j.cattod.2019.06.010.

[29] A.P. Ryaguzov, A.R. Assembayeva, M.M. Myrzabekova, et al., Study of the influence of palladium nanoparticles on the structure of DLC films synthesized on silicon (100) substrates, Diam. Relat. Mater. 126 (2022) 109125, https://doi.org/10.1016/j.diamond.2022.109125.

[30] K. Otto, C.P. Hubbard, W.H. Weber, G.W. Graham, Raman spectroscopy of palladium oxide on γ-alumina applicable to automotive catalysts: nondestructive, quantitative analysis; oxidation kinetics; fluorescence quenching, Appl. Catal. B Environ. 1 (1992) 317–327, https://doi.org/10.1016/0926-3373(92)80056-6.

[31] A. Baylet, P. Marécot, D. Duprez, et al., In situ Raman and in situXRD analysis of PdO reduction and Pd° oxidation supported on γ-Al2O3 catalyst under different atmospheres, Phys. Chem. Chem. Phys. 13 (2011) 4607–4613, https://doi.org/10.1039/C0CP01331E.
[32] M.D. Shultz, J.U. Reveles, S.N. Khanna, E.E. Carpenter, Reactive nature of dopamine as a surface functionalization agent in iron oxide nanoparticles, J. Am. Chem. Soc. 129 (2007) 2482–2487, https://doi.org/10.1021/ja0651963.
[33] N.F. Domancich, S.A. Fuente, A.C.R. Fernández, et al., Significance of different dopamine species as reducing agents of graphene oxide: fundamental aspects, Surf. Sci. 732 (2023) 122285, https://doi.org/10.1016/j.susc.2023.122285.
[34] A.R. Lopes da Silva, A. Jhones dos Santos, C.A. Martínez-Huitle, Electrochemical measurements and theoretical studies for understanding the behavior of catechol, resorcinol and hydroquinone on the boron doped diamond surface, RSC Adv. 8 (2018) 3483–3492, https://doi.org/10.1039/C7RA12257H.